

OPTIMIZATION OF THE SYNCHRONIZATION BANDWIDTH OF RATIONALLY SYNCHRONIZED OSCILLATORS BASED ON BIFURCATION CONTROL

M. Fernandez*, S. Ver Hoeye, C. Vazquez, G. Hotopan, R. Camblor, and F. Las Heras

Area of Signal Theory and Communications, Department of Electrical Engineering, University of Oviedo, Campus de Viesques, Edificio Polivalente s/n, Modulo 8, Planta 1, E-33203, Gijon, Spain

Abstract—In this work, a nonlinear technique for the optimization of the synchronization bandwidth of Rationally Synchronized Oscillators (RSO) is presented. The circuit is forced to operate near a Hopf bifurcation point which is created around the frequency of the input reference signal. Under this operating regime, the reference signal is strongly amplified and the synchronization bandwidth of the circuit is considerably improved. A 5–3 GHz rationally synchronized oscillator has been optimized using the proposed method. The manufactured RSO provides a 5 MHz synchronization bandwidth with a reference signal power of -22 dBm, in good agreement with simulation results.

1. INTRODUCTION

In modern microwave communication systems, carrier signals with good frequency stability and phase noise properties are required. The generation of these signals is often solved by using synthesized oscillators [1]. However, when several carrier signals at different frequencies, with the same reference signal, are needed, the complexity and the cost of the system rapidly rises with the number of used synthesized oscillators. A different approach based on the use of Rationally Synchronized Oscillators (RSO) can be applied to optimize the system. With this alternative, the required number of RSO circuits are synchronized with the same reference signal, provided by only one

Received 20 June 2011, Accepted 2 August 2011, Scheduled 8 August 2011

* Corresponding author: Miguel Fernandez Garcia (mfgarcia@tsc.uniovi.es).

synthesized oscillator. Because all the RSO circuits share the reference signal, the rational relation r between the free running frequency f_o and the frequency of the reference signal f_r , expressed as $r = \frac{f_o}{f_r} = \frac{M}{N}$, is different. With this configuration, all the RSO output signals have a known fixed phase relation with the reference signal, which can be of interest in some applications, while its phase noise inherits the properties of the reference signal.

The RSO proposed in this paper is based on a single transistor and a few number of components, and it is implemented in microstrip technology. Therefore, it is a power efficient, very compact and low cost circuit, which can be easily integrated with radiating elements, as a part of low cost active antennas [2–4]. However, the main drawback of RSO circuits is that they present very reduced synchronization bandwidth when the synchronization order is high, $M, N > 2$. This problem is greater if the synchronization signal power is relatively low, as occurs when several RSO share one reference signal. In that case, the synchronization phenomenon is only observable through the detection of noisy bumps [5] and the circuit has no practical interest.

In order to improve the locking range of fundamentally synchronized oscillators and fractional frequency dividers (RSO), when using low reference signal power, some techniques have been described in technical literature [6, 7]. They are based on the addition of low frequency feedback loops to the circuit, requiring additional circuitry and increasing the system complexity.

This work presents a new technique for the optimization of the locking range of high order RSO circuits. The operating regime of the circuit is forced to be near a Hopf bifurcation point, which is created around the frequency of the input reference signal. The amplification phenomenon associated to this particular operating point is used to enlarge the reference signal power and, consequently, the locking range of the circuit. Due to the high magnitude of the generated amplification effect, the required input reference signal power is considerably reduced, even for high order synchronization processes.

The proposed technique has been applied to the optimization of a 5–3 GHz RSO circuit with rational ratio $r = \frac{M}{N} = \frac{3}{5}$, in which the 5th harmonic component of the self-oscillation signal ($f_o = 3$ GHz, $N = 5$) synchronizes with the 3rd harmonic component of the input reference signal ($f_r = 5$ GHz, $M = 3$), generated due to the nonlinear characteristic of the active device.

The synchronization ranges of several RSO circuits whose operating point is located at different distances of the bifurcation point are analyzed by tracing the corresponding synchronization loci, as a

function of the input reference signal power, through harmonic balance techniques [7–10]. From this analysis, the best circuit is selected and manufactured, in order to validate the proposed optimization method.

The paper is organized as follows. In Section 2, the circuit topology and the design process are described and the proposed optimization method is presented. In Section 3 the locking range analysis technique used is outlined and the simulation results obtained after the optimization stage are presented and discussed. Section 4 provides some important details about the circuit implementation and shows the experimental characterization of the manufactured RSO, including phase noise measurements.

2. DESIGN AND OPTIMIZATION OF THE RSO

2.1. Topology

The circuit topology is represented in Fig. 1. It is based on a single ATF-36077 PHEMT transistor with a feedback network placed at the source port. This network enables the existence of a self-oscillation signal, with frequency $f_o = 3$ GHz, and includes a varactor diode to slightly modify the free running frequency. The input reference signal, with frequency $f_r = 5$ GHz, power P_r and arbitrary phase ϕ_r , is connected to the gate port of the transistor through a band-pass filter with center frequency f_r . Another band-pass filter with center frequency f_o is placed at the drain port of the transistor to select the output signal. At the gate port of the transistor it is also connected a multi-harmonic load $Z_L(f)$ based on an arbitrarily width modulated microstrip transmission line [11]. On the one hand, the multi-harmonic load allows the control of the frequency and the harmonic content of the self-oscillation signal. On the other hand, it will be used to set the operating point of the circuit in order to optimize the synchronization bandwidth, for a given value of the input signal power P_r . In addition, it is also used to fix the value of the quality factor of the oscillator during the entire optimization process.

2.2. Design

In a rationally synchronized oscillator with rational ratio $r = \frac{M}{N}$, the N th harmonic component of the self-oscillation signal synchronizes with the M th harmonic component of the input reference signal, which is generated due to the nonlinear characteristic of the active device. This synchronization regime presents common features with harmonic ($M = 1$) [6, 7, 12, 13], and with sub-harmonic synchronization ($N = 1$) [14, 15]. Therefore, for a given value of the reference signal power,

the synchronization range depends on the harmonic content and the quality factor of the circuit [16].

Although the high efficiency demonstrated by some analytical techniques developed for the analysis of nonlinear microwave circuits [17] and for the determination of the frequency, the amplitude [18–20] and the stability of the autonomous signal in oscillator circuits [21, 22], they are not useful in this case because it is not possible to obtain an analytical description of the RSO. Here, the frequency $f_o = f_{AG}$ and the amplitude of the fundamental harmonic $V_o^1 = V_{AG}$ are imposed through an optimization process, based on the technique of the auxiliary generator, in which several parameters of the circuit are modified in order to satisfy the non perturbation condition [8]. In addition, this method allows the control of the harmonic content of the self-oscillation signal. Thus, the optimum value of the amplitude of the N th harmonic component of the self-oscillation signal V_o^N can be also enforced.

Assuming a constant value of the input signal power, the amplitude of their M th harmonic component is determined by the nonlinear characteristic of the active device and the impedance of the multi-harmonic load $Z_L(f = M \times f_r)$. Despite of the good performance demonstrated by the harmonic optimization technique described in [16], when high synchronization order is considered, with $M > 2$, a relatively high value of the reference signal power is required in order to get a value of V_r^M enough to obtain a synchronization range usable in practice.

The third circuit characteristic that determines the synchronization bandwidth is the oscillator quality factor, which is defined as [23]:

$$Q = \frac{f_o}{2G_L} \frac{\partial Y_{AG}^i}{\partial f} \quad (1)$$

where G_L is the load conductance and Y_{AG}^i represents the frequency dependent imaginary part of the admittance evaluated at the gate port of the transistor. The value of Q is fixed maintaining constant these two terms throughout the entire optimization process.

2.3. Optimization Based on Bifurcation Control

Bifurcation theory is a powerful tool, since it provides a deep knowledge about the dynamics of nonlinear systems [24]. When the operation regime of a nonlinear circuit is near to a Hopf bifurcation point, an amplification phenomenon which affects to all the signals in the circuit is generated. This effect has been described in [5] as undesired, since it causes noise amplification over some spectral bands. However, in [25]

it is shown that it can be exploited and controlled to strongly amplify a weak signal.

The Hopf bifurcation point can be detected from the analysis of the transfer function of the system, which is linearized around its steady state solution. At the bifurcation point, a couple of complex conjugate poles, with negative real part, crosses the imaginary axis of the complex plane, invalidating the actual solution. The associated amplification effect is centered at the frequency of the couple of poles, and its magnitude increases as the negative real part of the poles decreases.

The desired operation regime is imposed by optimizing several parameters of the circuit in order to reach a quasi-zero admittance at the gate port of the transistor, where is connected the auxiliary generator. This condition must be satisfied around the frequency of the input reference signal, and it can be expressed as:

$$\begin{cases} Y_{AG}^r(f = f_r) = Y_L^r(f = f_r) + Y_{NL}^r(f = f_r) = \epsilon^r \approx 0 \\ Y_{AG}^i(f = f_r) = Y_L^i(f = f_r) + Y_{NL}^i(f = f_r) = \epsilon^i \approx 0 \end{cases} \quad (2)$$

where $Y_{AG}(f)$ is the admittance seen by the auxiliary generator and superscripts r and i are used to denote the real and the imaginary parts. Hence, it can be expressed as the sum of the admittances that represent the linear and the nonlinear part of the circuit (see Fig. 1). The optimization of the multi-harmonic load provides a precise control of the position of the couple of poles created after satisfying the condition imposed by (2). Thus, several operating points, associated to different values of amplification, can be reached.

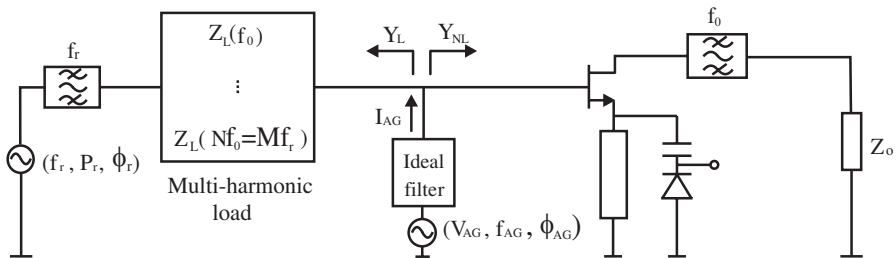


Figure 1. Topology of the rationally synchronized oscillator.

3. SYNCHRONIZATION RANGES OF THE RSO

For the analysis of the synchronization range of the RSO, a single-tone harmonic balance is implemented, with fundamental frequency $f_b = \frac{f_o}{M} = \frac{f_r}{N} = 1 \text{ GHz}$, taking into account $M \times N$ harmonics. In

that frequency basis, the self-oscillation frequency is expressed as $f_o = f_{AG} = M \times f_b$, the reference signal frequency as $f_r = N \times f_b$, and the synchronizing harmonics are located at $M \times N \times f_b = 15 \times f_b = 15 \text{ GHz}$.

The synchronization loci represents the solutions of the circuit for which the frequency of the N th harmonic component of the self-oscillation signal and the M th harmonic component of the reference signal are the same, $N \times f_o = M \times f_r$ and, thus, the phase difference $\Delta\phi = \phi_{V_r^M} - \phi_{V_o^N}$ is constant in time. The loci are obtained carrying out a sweep in $\Delta\phi$ between 0° and 360° , calculating for each point the values of V_{AG} and f_{AG} for which the non perturbation condition of the auxiliary generator is satisfied [8]. However, if $\phi_{V_r^M}$ is kept constant, the sweep can be realized by changing $\phi_{V_o^N}$ between 0° and 360° , or $\phi_{V_o} = \phi_{AG}$ between 0° and $\frac{360^\circ}{N} = 72^\circ$.

Figure 2 shows the synchronization loci of four circuits with different operating points, and with a common value of the reference signal power, $P_r = -22 \text{ dBm}$. The couple of poles associated to each one has been depicted in Fig. 3. It is observed that the locking range increases as the negative real part of the complex conjugate pole pair approaches zero. This is due to the fact that the magnitude of the amplification experienced by the reference signal is higher when the operation regime is closer to the Hopf bifurcation point. Because of the synchronization loci have a similar inclination angle, the quality factor is almost the same in all cases.

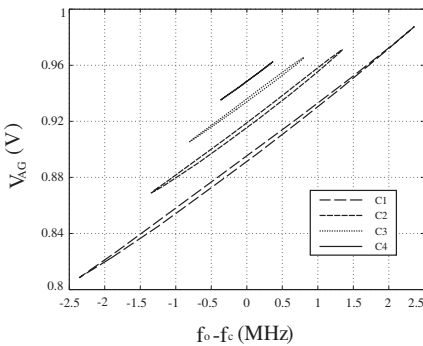


Figure 2. Synchronization loci of four circuits with different operation regimes. Each trace is normalized with respect to its central frequency f_c . The reference signal power is $P_r = -22 \text{ dBm}$ in all cases.

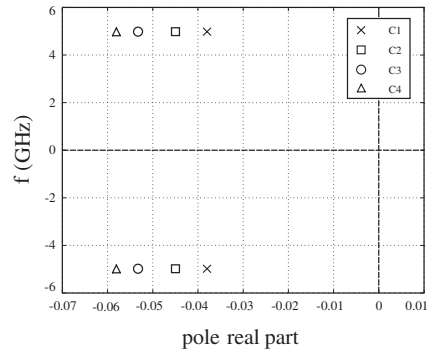


Figure 3. Complex conjugate poles associated to different operation regimes. Note that in all cases, the pole pair frequency is around f_r .

In Fig. 4, it has been represented the variation of the amplitude of the harmonic component V_{15} , with frequency $f_{15} = N \times f_o = M \times f_r$ along the synchronization loci of each circuit. Under synchronized operation, this signal can be expressed as the vectorial addition $\bar{V}_{15} = \bar{V}_o^N + \bar{V}_r^M$. Thus, its mean value represents the amplitude of the N th harmonic component of the self-oscillation signal, and its half peak to peak value is related to the amplitude of the M th harmonic component of the reference signal. As shown in Fig. 4, the value of V_o^N is similar in all cases, and the peak to peak value is higher when the operation point approaches to the bifurcation one.

Note that the quality factor, the amplitude of the N th harmonic component of the self-oscillation signal V_o^M and the power of the reference signal are the same in all the circuits. Hence, the synchronization range depends only on the proximity of the operation regime of each circuit to the bifurcation point.

The behavior of the synchronized solutions versus the reference signal power is analyzed by tracing the Arnold tongues of the RSO. This representation is achieved by drawing the frequency corners of the locking range as a function of the reference signal power. This information is contained in Fig. 5, in which the Arnold tongues of the RSO circuits corresponding with the circuits presented in Fig. 2 have been represented together with the Arnold tongue of a reference RSO without amplification effect. As the operation regime of the RSO approaches to the bifurcation point, the synchronized solutions shift to lower power, retaining its shape. This analysis shows that

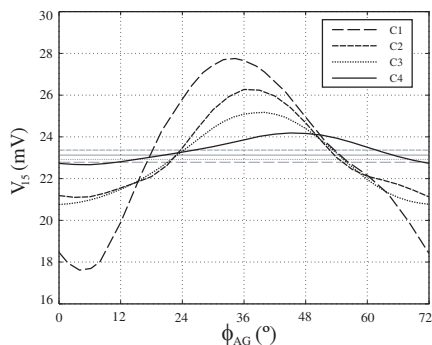


Figure 4. Amplitude of the signal \bar{V}_{15} at $M \times f_o = N \times f_r = 15$ GHz in synchronized operation. Grey lines: mean values of corresponding \bar{V}_{15} .

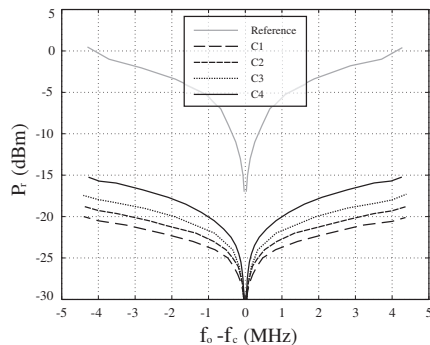


Figure 5. Arnold tongues of the four circuits with different operation regimes. Grey line: Arnold tongue of the reference circuit in which no input signal amplification effect is considered.

the operation regime selected works as an ideal amplifier whose gain is easily controllable, while other working parameters of the circuit remain constant. Note that, after the optimization, the reference signal power which is required to achieve a given synchronization bandwidth, can be reduced up to 20 dB.

4. IMPLEMENTATION AND EXPERIMENTAL RESULTS

In order to validate the proposed technique, the circuit with lowest input power, corresponding with C1 trace in Fig. 2, has been manufactured in microstrip technology. The selected substrate is ARLON 25N, with relative dielectric constant $\epsilon_r = 3.38$. All the passive elements, i.e., multi-harmonic load, filters and DC-bias and feedback networks has been implemented using distributed elements.

Despite the effort accomplished in order to develop precise models of transmission lines, their implementation in commercial software still has some effects which are not taken into account and can affect to the behavior of the implemented circuit [26]. In order to optimize the design process, at its final stage the frequency response of all the passive sub-networks has been calculated in an electromagnetic simulation based on the Method of Moments. Although the great electrical size of the considered structures, the required time in order to compute their frequency response can be significantly reduced by applying some efficient acceleration techniques [27, 28]. The information provided by this analysis has been used to slightly correct such networks in order to avoid undesired impedance deviations which could affect to the circuit performance.

4.1. Multi-Harmonic Load Implementation

Multi-harmonic load $Z_L(f)$ parameters are used along the entire design and optimization process in order to set and fix the desired values of the frequency and harmonic content of the self-oscillation signal and the quality factor of the oscillator. Its input impedance also determines the operation regime, since it needs to be modified in order to satisfy the condition imposed by (2). Therefore, it is necessary to have precise control over it at frequencies f_o , f_r , $N \times f_o$ and $M \times f_r$. Traditional implementations based on open ended stubs and microstrip lines can not be easily used for the desired purpose, because its frequency response is dominated by resonance phenomena. Thus, they are narrow band structures and the value of its impedance can not be controlled in a precise way.

The multi-harmonic load proposed in this work is based on an arbitrarily width modulated microstrip line [11]. The structure of the load is shown in Fig. 6. The base element is a tapered microstrip line [29], with length Δl and lateral widths w_1 and w_2 . The load is formed from the serial connection of N_Z base tapered lines, thus, the set of parameters that defines the load is composed of the load length $L_Z = N_Z \times \Delta l$ and the width pairs of each base element.

The main advantage of the proposed structure is that allows a precise control of its input impedance at different frequencies. In

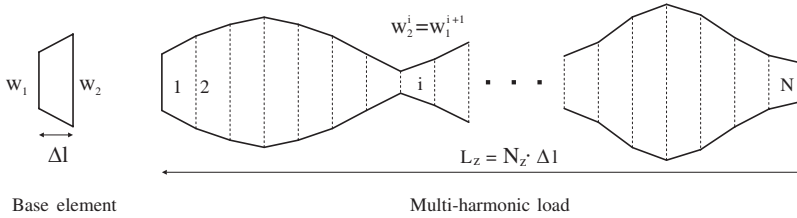


Figure 6. Scheme of the base element and arbitrarily modulated width transmission line.

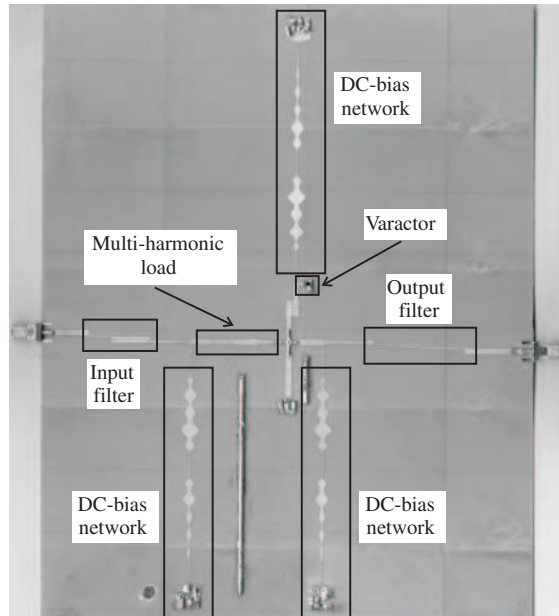


Figure 7. Picture of the manufactured 5–3 RSO prototype.

addition, this control can be applied over a relatively large bandwidth around each considered frequency point. These two features are also exploited in order to design the DC-bias networks. Note that, although other techniques for the design of compact and wide-band DC-bias structures have been developed [30], they can not provide the required input impedance control around all the considered harmonic components in the case of RSO circuits.

Figure 7 shows a picture of the manufactured RSO prototype, in which the final layout of the multi-harmonic load can be observed.

4.2. Experimental Results

The output power variation of the manufactured RSO circuit along the synchronization range, for different values of the reference signal power, has been represented in Fig. 8. In the same figure is also represented, in terms of the RSO output power, the simulated synchronization loci. Note that only half of the points contained on each synchronization loci are related to stable solutions. This set of points has been determined by means of envelope transient simulations [9, 10] and corresponds with the upper part of each loci. The measured variation of the locking range with respect to the power of the reference signal is shown in Fig. 9, and compared with simulation results. As can be observed from Figs. 8 and 9, a very good agreement is found between the simulated results and the experimental behavior of the manufactured RSO.

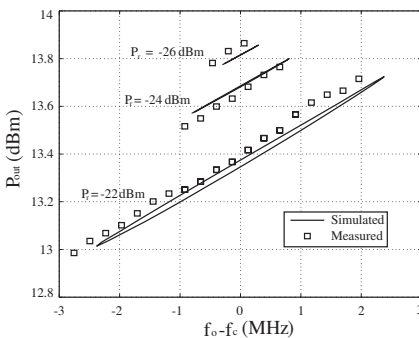


Figure 8. Comparison between simulated and measured variation of the output power along the locking range for different values of P_r .

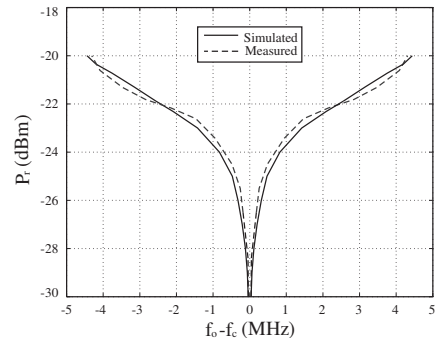


Figure 9. Measured synchronization range with respect to P_r .

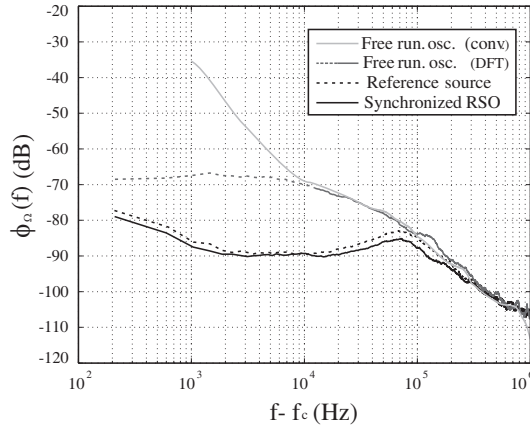


Figure 10. Comparison between the phase noise of the free-running oscillator, the rationally synchronized oscillator ($P_r = -20$ dBm) and the reference signal source. The dashed line corresponding to the free-running oscillator represents the invalid data provided by the DFT method.

Phase noise is a very relevant parameter that affects the performance of microwave systems [31, 32]. It has been experimentally characterized by means of a direct method. The frequency of the reference signal has been selected to ensure that the operating point of the RSO is about the center of the synchronization loci when its power is $P_r = -20$ dBm and the time variation of the output signal phase $\phi_{out}(t)$ has been measured. Then, the power spectral density $\Phi_{\Omega}(f)$ of the signal $\phi_{out}(t)$, calculated through a DFT, directly represents the phase noise evaluated at the out port of the RSO. The same procedure has been applied for the evaluation of the reference signal generator phase noise. In the case of free-running oscillator, the main contribution to the phase noise near to the carrier is the frequency variation of the autonomous signal [33]. Therefore, when no reference signal is considered, the described methodology is not valid near to the carrier because it assumes a constant frequency operation. In that frequency region, the phase noise of the free-running oscillator has been measured by means of commercial software based on the evaluation of the PN-AN conversion. The results are represented in Fig. 10. Note that the two proposed methods to evaluate the phase noise of the free-running oscillator provide identical results when the measurement frequency is far away from the carrier. Since the phase noise of the RSO follows that of the reference source, the rational synchronization process considerably improves the phase noise of the system.

5. CONCLUSION

A new technique for the optimization of the synchronization bandwidth of rationally synchronized oscillators has been presented. The amplification effect associated to the proximity of the circuit operation regime to a Hopf bifurcation point is exploited to amplify the input reference signal. The optimization of the multi-harmonic load based on an arbitrarily modulated width microstrip line provides a precise control over the magnitude of such effect. Several circuits, with the same harmonic content and quality factor, working at different distances of the bifurcation point, have been designed. It has been shown that the synchronization range increases when the operation regime approaches to the bifurcation point, since the generated amplification is larger. The best circuit has been manufactured and experimentally characterized, obtaining a good agreement with the simulation results. Phase noise measurement shows the improvement of this parameter in rationally synchronized operation.

ACKNOWLEDGMENT

This work has been supported by the Ministerio de Ciencia e Innovacion of Spain (FEDER) under projects TEC2008-01638, CONSOLIDER-INGENIO CSD2008-00068 and grant AP2009-0438, by the Gobierno del Principado de Asturias (PCTI/FEDER-FSE) under projects EQUIP08-06, FC09-COF09-12, EQUIP10-31 and PC10-06, grant BP10-031 and by Catedra Telefonica-Universidad de Oviedo.

REFERENCES

1. Myoung, S.-S., Y.-J. An, and J.-G. Yook, "A novel 10 GHz super-heterodyne bio-radar system based on a frequency multiplier and phase-locked loop," *Progress In Electromagnetics Research C*, Vol. 19, 149–162, 2011.
2. Garcia, J. A., L. Cabria, and R. Marante, "An unbiased dual-mode mixing antenna for wireless transponders," *Progress In Electromagnetics Research*, Vol. 102, 1–14, 2010.
3. Goel, P. and K. J. Vinoy, "A low-cost phased array antenna integrated with phase shifters cofabricated on the laminate," *Progress In Electromagnetics Research B*, Vol. 30, 255–277, 2011.
4. Vazquez Antuna, C., G. R. Hotopan, S. Ver Hoeye, M. Fernandez Garcia, L. F. Herran Ontanon, and F. Las-Heras Andrés,

- “Microstrip antenna design based on stacked patches for reconfigurable two dimensional planar array topologies,” *Progress In Electromagnetics Research*, Vol. 97, 95–104, 2009.
5. Ver Hoeye, S., A. Suarez, and S. Sancho, “Analysis of noise effects on the nonlinear dynamics of synchronized oscillators,” *IEEE Microwave and Wireless Components Letters*, Vol. 11, No. 9, 376–378, 2001.
 6. Chang, H. C., A. P. Yeh, and R. A. York, “Analysis of oscillators with external feedback loop for improved locking range and noise reduction,” *IEEE Microwave and Wireless Components Letters*, Vol. 47, No. 8, 1535–1537, 1999.
 7. Ramirez, F., E. De Cos, and A. Suarez, “Nonlinear analysis tools for the optimized design of harmonic-injection dividers,” *IEEE Transactions on Microwave Theory and Techniques*, Vol. 51, No. 6, 1752–1762, 2003.
 8. Ver Hoeye, S., L. Gutierrez, S. Sancho, A. Suarez, and P. Gonzalez, “Sub-harmonic and rational synchronization for phase-noise improvement,” *Proc. 31st Eur. Microw. Conference*, Vol. 1, No. 1, 237–240, 2001.
 9. Ver Hoeye, S., L. F. Herran, M. Fernandez, and F. Las Heras, “Design and analysis of a microwave large-range variable phase-shifter based on an injection-locked harmonic self-oscillating mixer,” *IEEE Microwave and Wireless Components Letters*, Vol. 16, No. 6, 342–344, 2006.
 10. Vazquez, C., S. Ver Hoeye, M. Fernandez, L. F. Herran, and F. Las Heras, “Analysis of the performance of injection locked oscillators in a data transmitting polarisation agile antenna application,” *Progress In Electromagnetics Research Letters*, Vol. 12, 1–10, 2009.
 11. Ver Hoeye, S., C. Vazquez, M. Gonzalez, M. Fernandez, L. F. Herran, and F. Las Heras, “Multi-harmonic DC-bias network based on arbitrarily width modulated microstrip line,” *Progress In Electromagnetics Research Letters*, Vol. 11, 119–128, 2009.
 12. Ramirez, F., M. Ponton, S. Sancho, and A. Suarez, “Phase-noise analysis of injection-locked oscillators and analog frequency dividers,” *IEEE Transactions on Microwave Theory and Techniques*, Vol. 56, No. 2, 393–407, 2008.
 13. Schmideg, I., “Harmonic synchronization of nonlinear oscillators,” *Proceedings of the IEEE*, Vol. 59, No. 9, 1250–1251, 1971.
 14. Zhang, X., X. Zhou, and A. S. Daryoush, “A theoretical and experimental study of the noise behavior of subharmonically injection locked local oscillators,” *IEEE Transactions on Microwave*

- Theory and Techniques*, Vol. 40, No. 5, 895–902, 1992.
15. Kudsus, S., T. Berceci, A. Tessmann, M. Neumann, and W. H. Haydl, “W-band HEMT oscillator MMICs using subharmonic injection locking,” *IEEE Transactions on Microwave Theory and Techniques*, Vol. 48, No. 12, 2526–2532, 2000.
 16. Ver Hoeye, S., M. G. Corredoiras, M. Fernandez, C. Vazquez, L. F. Herran, and F. Las Heras, “Harmonic optimization of rationally synchronized oscillators,” *IEEE Microwave and Wireless Components Letters*, Vol. 19, No. 5, 317–319, 2009.
 17. Lee, K.-C. and C.-W. Huang, “Analysis of nonlinear microwave circuits by particle swarm algorithm,” *Journal of Electromagnetic Waves and Applications*, Vol. 21, No. 10, 1353–1365, 2007.
 18. Gonzalez-Posadas, V., J. L. Jimenez-Martin, A. Parra-Cerrada, D. Segovia-Vargas, and L. E. Garcia-Munoz, “Oscillator accurate linear analysis and design. Classic linear methods review and comments,” *Progress In Electromagnetics Research*, Vol. 118, 89–116, 2011.
 19. Ganji, S. S., D. D. Ganji, and S. Karimpour, “Determination of the frequency-amplitude relation for nonlinear oscillators with fractional potential using He’s energy balanced method,” *Progress In Electromagnetics Research C*, Vol. 5, 21–33, 2008.
 20. Akbarzade, M., D. D. Ganji, and H. Pashaei, “Analysis of nonlinear oscillators with u^n force by He’s energy balance method,” *Progress In Electromagnetics Research C*, Vol. 3, 57–66, 2008.
 21. Vahdati, H. and A. Abdipour, “Nonlinear stability analysis of an oscillator using the periodic averaging method,” *Progress In Electromagnetics Research*, Vol. 79, 179–193, 2008.
 22. Vahdati, H. and A. Abdipour, “Nonlinear stability analysis of an oscillator with distributed element resonator,” *Progress In Electromagnetics Research*, Vol. 80, 241–252, 2008.
 23. Combes, P. F., J. Graffeuil, and J. F. Sautereau, *Microwave Components, Devices and Circuits*, Wiley, New York, 1987.
 24. Makeeva, G. S., O. A. Golovanov, and M. Pardavi-Horvath, “Mathematical modeling of nonlinear waves and oscillations in gyromagnetic structures by bifurcation theory methods,” *Journal of Electromagnetic Waves and Applications*, Vol. 20, No. 11, 1503–1510, 2006.
 25. Fernandez, M., S. Ver Hoeye, L. F. Herran, and F. Las Heras, “Nonlinear optimization of wide-band harmonic self-oscillating mixers,” *IEEE Microwave and Wireless Components Letters*,

- Vol. 18, No. 5, 347–349, 2008.
26. Xie, H., J. Wang, R. Fan, and Y. Liu, “Study of loss effect of transmission lines and validity of a Spice model in electromagnetic topology,” *Progress In Electromagnetics Research*, Vol. 90, 89–103, 2009.
 27. See, K. Y., E. K. Chua, and Z.-H. Liu, “Accurate and efficient evaluation of MoM matrix based on a generalized analytical approach,” *Progress In Electromagnetics Research*, Vol. 94, 367–382, 2009.
 28. Gurel, L., O. Ergul, A. Unal, and T. Malas, “Fast and accurate analysis of large metamaterial structures using the Multilevel Fast Multipole algorithm,” *Progress In Electromagnetics Research*, Vol. 95, 179–198, 2009.
 29. Chiang, C. T. and B.-K. Chung, “Ultra wideband power divider using tapered line,” *Progress In Electromagnetics Research*, Vol. 106, 61–73, 2010.
 30. Ma, J., T. Jing, and Y.-Z. Yin, “Compact and wideband DC bias line based on defected ground structure,” *Journal of Electromagnetics Waves and Applications*, Vol. 24, No. 4, 435–443, 2010.
 31. Park, C., H. Seo, and B. Kim, “A noise optimized passive mixer for charge-domain sampling applications,” *Journal of Electromagnetics Waves and Applications*, Vol. 23, No. 14–15, 1909–1917, 2009.
 32. Wu, T., H. Tang, and F. Xiao, “Research on the coherent phase noise of millimeter-wave doppler radar,” *Progress In Electromagnetics Research Letters*, Vol. 5, 23–34, 2008.
 33. Suarez, A., S. Sancho, S. Ver Hoeye, and J. Portilla, “Analytical comparison between time- and frequency-domain techniques for phase-noise analysis,” *IEEE Transactions on Microwave Theory and Techniques*, Vol. 50, No. 10, 2353–2361, 2002.